Proceedings of the Institution of Civil Engineers
Construction Materials 160
May 2007 Issue CM2
Pages 57–63
doi: 10.1680/coma.2007.160.2.57

Paper 07-00020
Received 17/07/2007
Accepted 30/07/2007

Keywords:
research & development/
strength & testing of materials/
sustainability

Richard J. Ball
Materials Scientist,
Interface Analysis Centre,
University of Bristol, UK

Adel El-Turki
Chemist,
Interface Analysis Centre,
University of Bristol, UK

William J. Allen
Consulting Engineer,
Ellis and Moore Consulting
Engineers, Bath, UK

Geoffrey C. Allen
Professor,
Interface Analysis Centre,
University of Bristol, UK

ice
Institution of Civil Engineers

The stress cycling of hydraulic lime mortars

R. J. Ball BEng, PhD, CSci, MIMMM, A. El-Turki MSc, PhD, W. J. Allen BEng, PhD, CEng, MICE and G. C. Allen BSc, PhD, DSc, CChem, FRSC

The effect of thermal expansion and contraction in masonry has been simulated using repeated stress cycles. Cylindrical specimens cast from 1:2 NHL3.5 lime mortar were exposed to air at 20°C and 65% relative humidity with a CO_2 concentration of 400 ppm for 28 and 84 days respectively prior to stress cycling 40 times. Cycling did not influence the peak stress recorded from subsequent destructive compressive testing, however the un-cycled specimens absorbed more energy up to the peak stress, compared with the cycled specimens. Ion-induced electron images of the mortar structure revealed the presence of micro-cracks in the cycled mortars, suggesting the energy absorbing mechanism.

1. INTRODUCTION

Lime mortars have been used in construction for thousands of years but in the last century ordinary Portland cement (OPC) became the predominant cementitious binder in most applications.[1] The high strength of OPC combined with relatively short setting times has allowed architects and engineers to design larger structures and reduce the construction time. However, mortars manufactured using OPC exhibit negligible plastic deformation under load and fail by brittle fracture. This can lead to the development of large internal stresses within a structure that are often dissipated by the formation of unsightly cracks and a reduction in strength. In a number of cases historic buildings have been damaged by inappropriate use of cement during repair.

Greater environmental awareness of the advantages of lime mortars in terms of carbon dioxide emissions released during their manufacture and the adsorption of carbon dioxide during carbonation is promoting a resurgence in their use. The ability of lime mortars to accommodate movement can alleviate the use of expansion joints in a structure.

Lime mortars harden by carbonation, in the case of a calcium lime mortar, or a combination of hydration and carbonation, as in hydraulic lime mortars. In hydraulic mortars the initial hydration reaction results in the formation of a C–S–H (calcium–silicate–hydrate) structure, which provides an initial set.[2,3] The remaining calcium hydroxide then carbonates over time. For the carbonation reaction to occur, carbon dioxide must diffuse into the mortar to form carbonic acid, which subsequently carbonates the remaining calcium hydroxide. The increase in volume associated with carbonation fills surface pores and cracks, reducing the number of diffusion paths and restricting the diffusion of carbon dioxide to greater depths.[4] In thick-walled structures this will limit the extent of carbonation to mortar located at the centre of the wall.

The ability of lime mortars to accommodate movement is considered to be a consequence of their 'plastic' and 'self-healing' properties. Cracks may provide a route by which carbon dioxide diffuses into the mortar whereupon carbonation fills the void, restoring strength. If the mortar is fully carbonated, dissolution and reprecipitation of calcium carbonate caused by moisture movement through the structure may also contribute to strength being regained.[5] Reprecipitation of calcium hydroxide may also provide a mechanism by which reconfiguration can occur. These mechanisms are commonly associated with autogenous healing.

The omission of thermal expansion joints in modern construction has a number of advantages which appeal to architects and engineers. These include a reduction in cost and a more aesthetically pleasing finish. When omitting thermal expansion joints in a lime-built structure, however, consideration must be given to both the mechanical and chemical behaviour of the mortar in service. Due to differences in the geometry, material properties, and diffusion of moisture and carbon dioxide throughout a structure, it is highly improbable that a thick solid wall will behave in a similar way to a thin cavity wall. In the context of this paper a thick wall would be considered as having a thickness in excess of 215 mm whereas the outer skin of a typical thin cavity wall would be 103 mm.

The results presented in this paper form part of a larger study investigating a wide range of lime mortar properties including, among other things, weathering and creep behaviour. Due to the nature of this work there are limited standards by industry experts for testing lime mortars and indeed many of these are viewed by industry experts as inappropriate or deficient in some respects. An explanation for this is that many have been adapted directly from existing cement standards and do not address many of the fundamental differences.

Here we report a study of the changes occurring in a mortar subjected to repeated stress cycles to simulate the effect of thermal expansion and contraction. Characterisation of the microstructure and chemical composition was undertaken using

Chemical composition: % w/w	NHL3.5
SiO_2	10·5
Al_2O_3	3·8
Fe_2O_3	1·5
CaO	60·9
MgO	1·5
K_2O	0·93
Na_2O	0·11
SO_3	1·43
Cl	0·01
Loss on ignition	20·2
Total	100·91
Insoluble residue	0·9
Calcinations loss	9·2
Soluble SO_3	0·52
Relative density: kg/m^3	—
Soluble SiO_2	—
C_2S	25·0
$Ca(OH)_2$	38·1
$CaCO_3$	20·9
$CaSO_4$	0·9
C_4AF	4·5
C_3A	3·8
C_2AS	3·9
Total	98·0
Cementation index	0·51

Table 1. Chemical composition of NHL3.5 lime as received

focused ion beam imaging. Specimens were conditioned in a controlled environment before their subjection to a stress cycling regime to simulate the repeated loading and unloading of a mortar. They were then destructively tested in compression.

2. EXPERIMENTAL METHOD

2.1. Specimen manufacture and exposure

Specimens were manufactured from a batch of natural hydraulic lime (NHL3.5) from Hydraulic Limes Ltd. The chemical analysis is given in Table 1. Croxden sand of grading shown in Fig. 1 was used as aggregate in the specimen preparation. Particles greater than 5 mm in size were removed, producing a cylinder diameter to maximum sand particle size ratio of 3·6. The lime/sand ratio was 1:2 by volume. Water was added to provide a mix flow of between 180 to 200 mm and a Hobart mixer was used to mix the lime, sand and water for a duration of 10 min. The mould was coated with release oil prior to casting the lime–sand mixture into cylinders of diameter 18 mm and length 36 mm. This specimen size was specified to ensure that significant

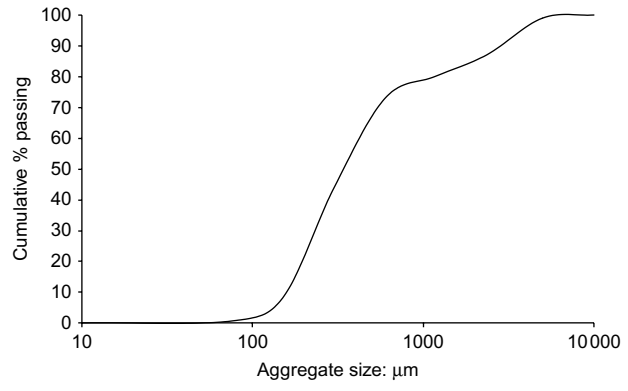

Fig. 1. Croxden sand aggregate grading

carbonation of the entire volume of the specimen could be achieved within the timescales available for specimen exposure and testing.

Results from previous testing programmes using this cylindrical sample geometry demonstrated its ability to provide consistent and reproducible results.[6] When a comparison was made with BS EN 196-1[7] 40 mm × 40 mm prisms, changes in the absolute value recorded for compressive strength were observed for some mixes. In the context of this paper this does not prejudice the results, which are principally concerned with the energies absorbed during stress cycling and the effect on compressive strength.

To reduce the presence of air pockets within the specimens and to ensure an even distribution of lime mix within the mould, each mould was half-filled and vibrated for 1 min before filling the mould to just below the top and continuing vibration for a further 1 min. A thin layer of high alumina cement was then applied to the top of each specimen and smoothed to ensure that the top surface of each cylinder was flat and parallel with the bottom surface. The specimens were then left under the laboratory conditions of 25°C and 50% relative humidity to harden. To ease extraction of the specimens the mould had a removable bottom and was split along the specimen length. After one day the bottom of the mould was removed and after six days the mould was separated to remove the cylindrical specimens.

Following de-moulding the specimens were placed in a Slimline 450 environmental chamber, manufactured by Sharetree Systems, at a temperature of 20 ± 1°C and relative humidity of 65 ± 1%. Specimen selection was randomised to reduce the effects of any systematic errors. Carbon dioxide gas from a cylinder was passed into the chamber to allow levels to be maintained at a constant value and to replace carbon dioxide removed by carbonation. Carbon dioxide levels in the chamber used in this study were held at 400 ± 50 ppm (parts per million) and monitored using an Edinburgh Instruments GascardII*plus* carbon dioxide detector set at 0–2000 ppm. The variables represent, within acceptable limits, a typical exposure condition in a building. These conditions are controlled variables, which were maintained to enable conduction of fair tests on selected dependent variables. Specimens were exposed in the chambers for durations of 28 and 84 days. A total of 10 specimens were tested at each treatment condition.

2.2. Stress cycling and mechanical testing

The compressive strength of each specimen was determined using a Zwick/Rowell testing machine with 10 kN load cell with resolution of 0·1 N. It was possible to determine displacements from the machine cross-head movement as the high machine stiffness and relatively low forces employed ensured that errors introduced from deflection of the machine were negligible. The specimen was mounted between two parallel stainless steel platens. The top platen was allowed to pivot on a ball joint to accommodate irregularities in the specimens. Loading was applied at a constant stress rate of 0·079 N/mm^2 per s (MPa/s) until the ultimate stress was reached. For each set of specimens tested, the average ultimate stress, $\sigma_{\text{average ultimate}}$, and standard deviation, s, was calculated.

Repeated application of stress on the mortar specimens was achieved using the same specimen and machine geometry as for the

quasi-static compressive tests described above. The testing machine was programmed to automatically load and unload the specimen 40 times. Loading was carried out under a force-controlled mode at a constant stress rate of 0·079 N/mm^2 per s (MPa/s) until a maximum value $\sigma_{cycling}$ was reached. The stress rate used for both cycling and destructive tests was sufficiently low to avoid the introduction of a dynamic response from the specimens. The cycling limits were defined as follows: a value of $\sigma_{cycling}$ for each set of specimens tested was calculated using equation (1)

$$\sigma_{cycling} = \sigma_{average\ ultimate} - s \quad (1)$$

where s is the standard deviation for the corresponding set of 10 specimens. When this value, $\sigma_{cycling}$, was reached during the first loading cycle, the specimens were unloaded at a constant strain rate of 10 mm/min until the strain equal to that at 20 N during the first cycle was obtained. This value was then used to define the lower load cycling limit for all subsequent cycles. Consequently a small number of samples from each batch failed during loading if their strength fell below the cycling stress.

2.3. Microstructural analyses

Microstructural examination of the specimens was carried out using an FEI FIB201 focused ion beam (FIB). The FIB instrument used a gallium ion beam of varying diameters and currents ranging from 1 pA to 12 nA, at 30 keV energy. A platinum organometallic gas injector was used for ion-assisted deposition of platinum over selected regions of the specimen to avoid electrical charging effects produced under ion bombardment. Secondary electrons, excited by the ion beam, were captured using a channel electron multiplier.

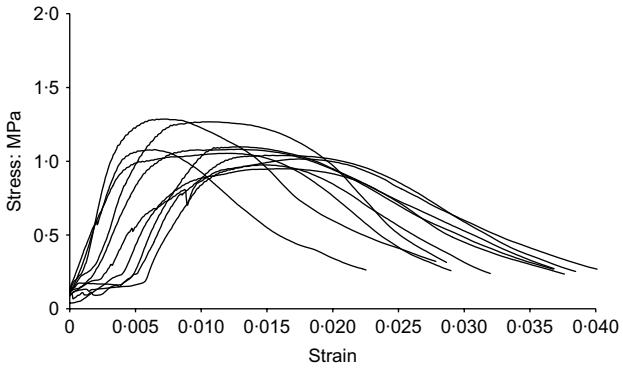

Fig. 2. Stress plotted against strain for specimens exposed for 28 days

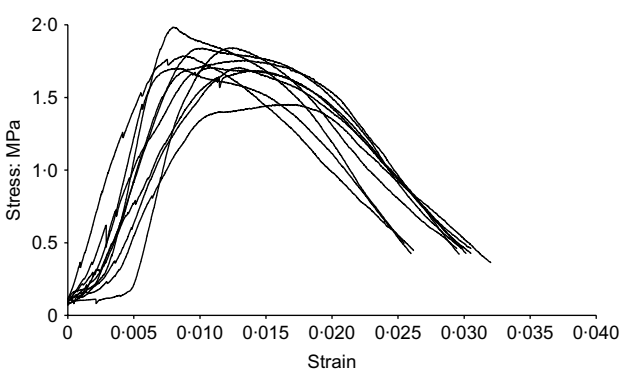

Fig. 3. Stress plotted against strain for specimens exposed for 84 days

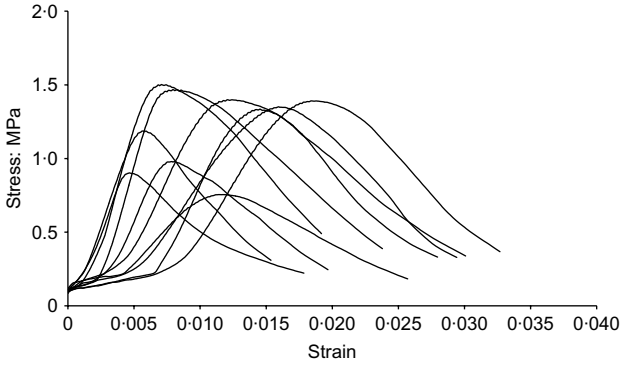

Fig. 4. Stress plotted against strain for specimens exposed for 28 days and subjected to 40 cycles

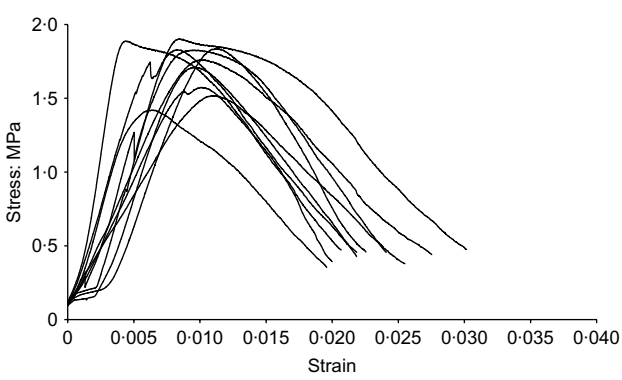

Fig. 5. Stress plotted against strain for specimens exposed for 84 days and subjected to 40 cycles

3. RESULTS AND DISCUSSION

3.1. Compressive testing and stress cycling

Figures 2 and 3 show plots of stress plotted against strain for each set of 10 specimens conditioned in the chamber for 28 and 84 days, respectively. Figs 4 and 5 show the equivalent data for specimens conditioned for 28 and 84 days respectively and cycled 40 times.

Figure 6 shows the average ultimate stress for cycled and uncycled specimens at 28 and 84 days exposure calculated from the ultimate stress (from the data) shown in Figs 2–5. The ultimate stress of the specimens aged for 84 days is noticeably higher than that of the specimens aged for 28 days irrespective of cycling conditions. This suggested that stress cycling had no effect on the compressive strength of specimens aged for 28 and 84 days.

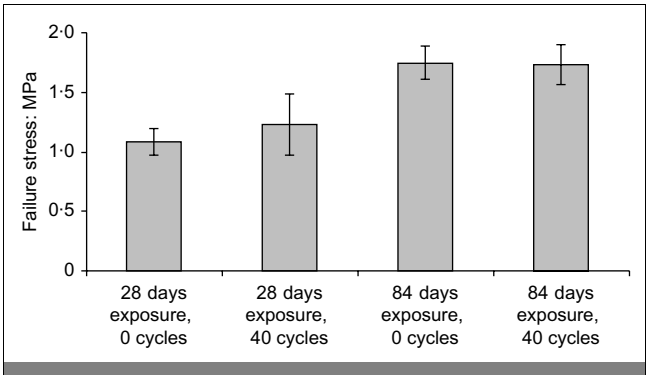

Fig. 6. Average ultimate stress for each set of specimens. Error bars show ± 1 standard deviation

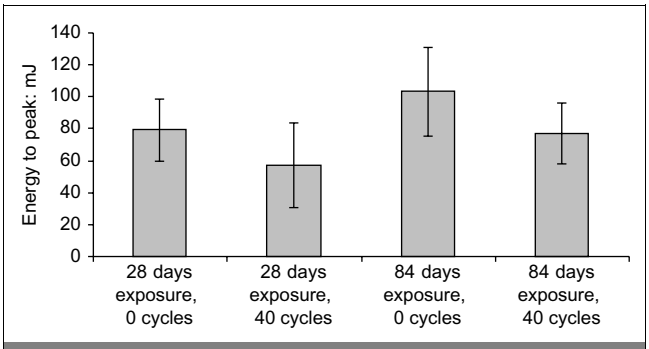

Fig. 7. Average energy adsorbed from the beginning of the test to the ultimate stress for each set of specimens. Error bars show ± 1 standard deviation

The energy absorbed during the compressive test up to the point of ultimate stress (maximum load) was calculated using equation (2) for each specimen tested, where F is the force applied and $\mathrm{d}x$ is the displacement.

$$\text{Energy} = \int F \mathrm{d}x \qquad (2)$$

It should be noted that where bedding-in occurrs the associated energy will be included. The contribution from bedding-in can be assumed to be small considering that: (*a*) the energy calculated is an average of 10 individual samples, not all of which had an initial bedding-in, and (*b*) the force at which bedding-in occurred was low compared to the maximum failure stress.

The average energy and standard deviation for each batch of specimens is shown in Fig. 7. The energy adsorbed was greater for the specimens aged for 84 days in comparison with those aged for 28 days. The energy adsorbed by the cycled specimens was also less than that for the uncycled specimens. This suggested that the energy adsorbed by the mortar during the cycling regime was dissipated by structural change.

Values of Young's modulus for each specimen tested was determined over a predefined number of data points along the linear section of the stress–strain curve with maximum gradient. Average values for each set of data were calculated and plotted in Fig. 8. Consideration of these data suggested that the specimen curing period was much more influential in determining the value of Young's modulus than cycling conditions.

For both the 28- and 84-day exposure, there was no significant difference in either the maximum stress or modulus, although

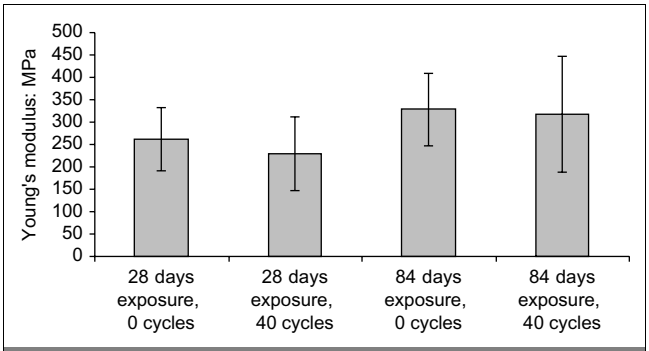

Fig. 8. Average Young's modulus for each set of specimens. Error bars show ± 1 standard deviation

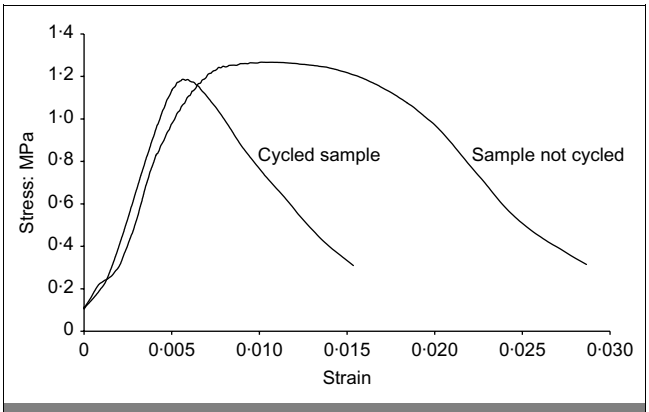

Fig. 9. Typical stress–strain plots for a cycled and non-cycled 28-day specimen showing difference in strain to ultimate stress

this was not the case for the energy absorbed to ultimate stress, in which the cycled specimens yielded a lower value. As the initial linear portions of the stress–strain curves were similar, it was evident that the observed differences resulted from a variation in behaviour around the ultimate stress event itself. Perusal of the curves suggested a more rounded shape for the uncycled specimens compared with a generally more acute profile for the cycled batches. This was examined in more detail with a systematic characterisation of the curve shapes.

The curves shown in Figs 2–5 contain a number of features that are characteristic of the lime mortars under test. The shape and dimensions of each part of the curve represented the way in which the specimen failed. The curvature at the top of the stress–strain plot for cycled specimens was in general sharper than that for the uncycled batch as can be seen in Fig. 9.

Figure 10 shows a typical stress–strain plot. Some specimens exhibited a small amount of strain before the force increased. This was due to localised crushing of surface irregularities (bedding-in) after which the curves followed a linear trend until just before the ultimate stress was reached. A value of Young's modulus was calculated for the linear section of the curve. Flattening occurred after the linear section leading to the maximum stress of the specimen, after which a decrease was observed.

To identify the effects of stress cycling on each set of specimens, a number of parameters were used. These are shown in Fig. 10. A method of calculating the strain to ultimate stress was developed

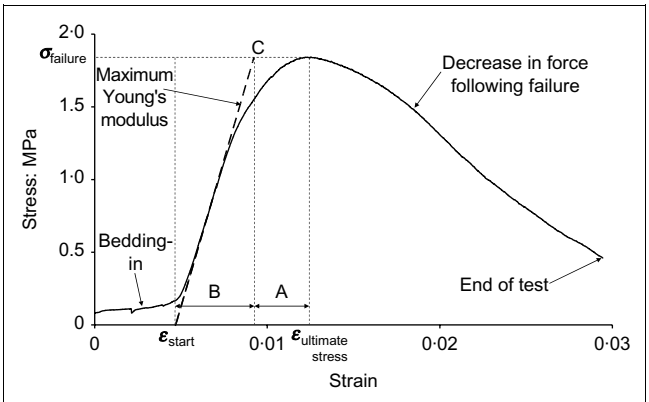

Fig. 10. Typical stress–strain plot for a lime mortar specimen

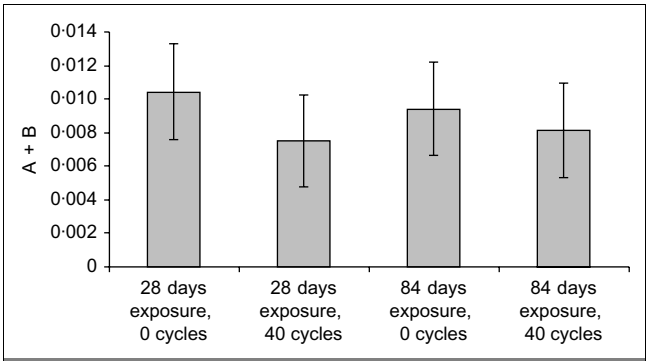

Fig. 11. Strain to ultimate stress excluding effects of bedding-in (A + B). Error bars show ± 1 standard deviation

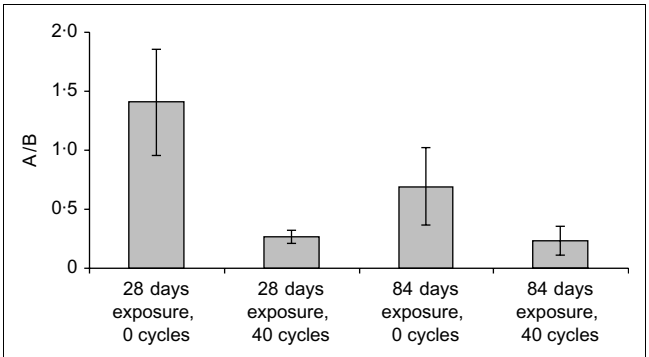

Fig. 12. Ratio of strain parameters A and B (A/B). Error bars show ± 1 standard deviation

using the position of the line drawn through the linear proportion of the curve. Extrapolation of this line to the point at which it intersected the strain axis was taken as the start of the test, ε_{start}, and used as the origin for subsequent analysis. A measure of the shape of the top proportion of the curve at ultimate stress was obtained by considering the strain at the point on the line corresponding to the ultimate stress, C. Parameters A and B corresponded to the strain between $\varepsilon_{ultimate\ stress}$ and C and ε_{start} and C respectively.

A modified strain to ultimate stress was obtained from the sum of A and B. This value eliminated effects from bedding-in. The value of A + B calculated for each set of specimens is shown in Fig. 11. This shows a smaller strain to ultimate stress for the cycled specimens.

As both the modulus and ultimate stress were assumed to be unaffected by cycling, the stress and strain represented by point C will be the same for each batch. The ratio A/B therefore gave an objective measure of differences in the shape of the curve approaching ultimate stress that was reflected in the energy absorbed. Fig. 12 shows the ratio of parameters A/B for each set of specimens. A decrease in the ratio for the cycled specimens indicates a dramatic decrease in the strain prior to ultimate stress, A.

3.2. Microstructural analyses

Figures 13(a) and (b) show ion-induced electron images obtained from the outer and internal fracture surfaces of a specimen aged for 28 days. Figure 13(a) shows sand grains bound together by a matrix of calcium carbonate crystals < 1 μm.

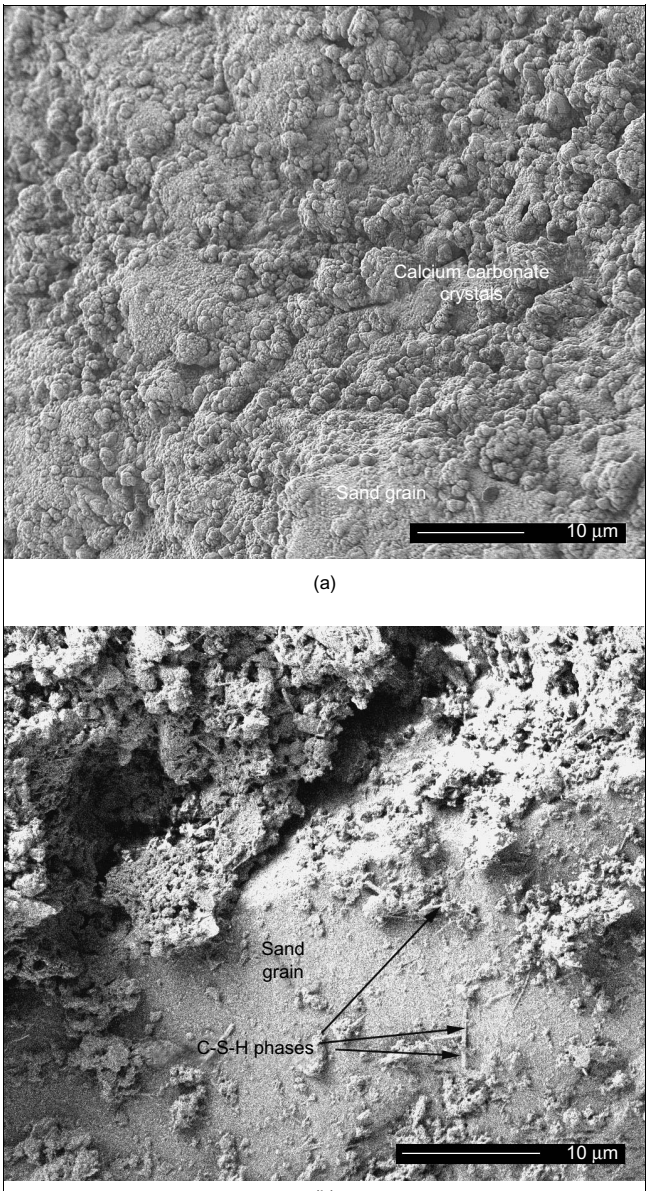

Fig. 13. Ion-induced electron images of lime mortar aged for 28 days: (a) showing the formation of calcite crystals on the surface; (b) fractured surface showing the presence of C–S–H

These formed small agglomerates with a maximum size of approximately 5 μm. The structure suggested intimate bonding between the sand particles and calcium carbonate matrix.

Examination of a fracture surface from the interior of the specimen (Fig. 13(b)), revealed a number of needle-like crystals of C–S–H distributed throughout the calcium carbonate matrix and at the surface of a sand particle.

The surface of a specimen aged for 84 days is shown in Fig. 14(a). Calcium carbonate crystals were observed to be of similar size and appearance to those on the 28-day specimen of Fig. 13(a).

Examination of the internal fracture surface (Fig. 14(b)) revealed a matrix of needle-like crystals of C–S–H. These were observed in much higher proportions than in the 28-day specimen. Angular plate-like crystals resembling portlandite were distributed throughout the matrix. The absence of these crystals in the 28-day specimens and the increased amount of C–S–H

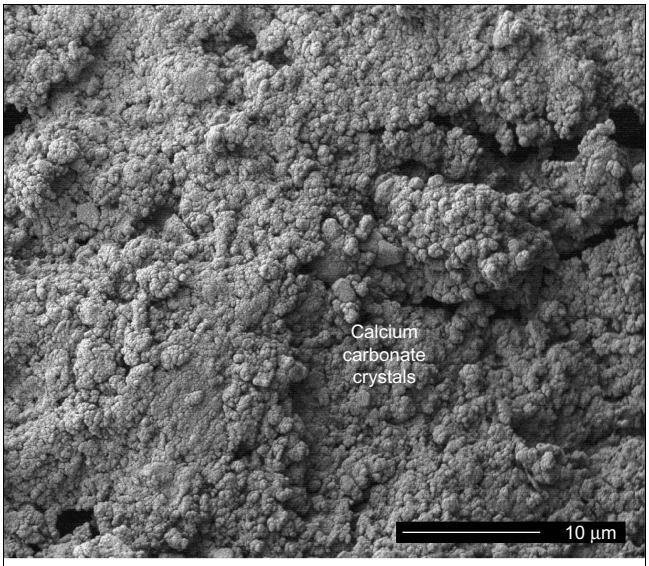

(a)

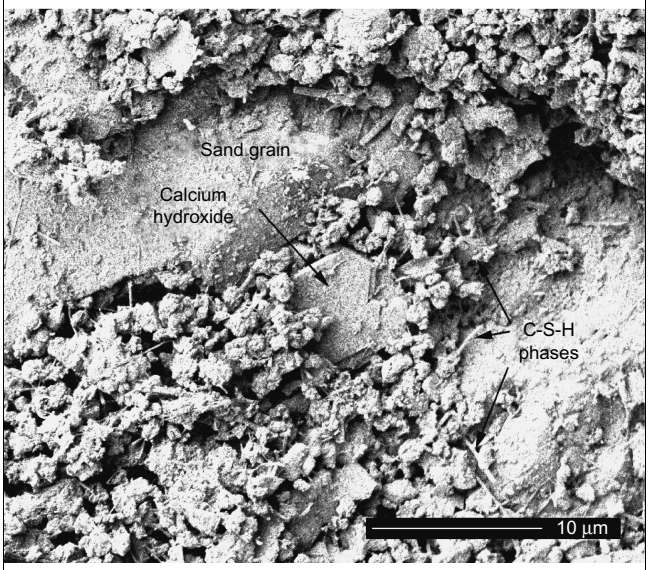

(b)

Fig. 14. Ion-induced electron images of lime mortar aged for 84 days: (a) showing the formation of calcite crystals; (b) fractured surface showing the presence of C–S–H and portlandite (CH)

phase suggested that their formation occurred during the hydration reaction (equation (3))[8]

$$2(2CaO \cdot SiO_2) + 4H_2O \rightarrow 3CaO \cdot 2SiO_2 \cdot 3H_2O + Ca(OH)_2 \quad (3)$$

Carbonation of calcium hydroxide would subsequently be expected via equation (4)

$$Ca(OH)_2 + CO_2 \rightarrow CaCO_3 + H_2O \quad (4)$$

The internal fracture surface of a stress-cycled specimen is shown in Fig. 15. The calcium carbonate matrix contained a large crack approximately 40 μm in width. Silicate crystals located on the internal surfaces of this crack indicated that it was not formed during stress cycling. A small microcrack approximately 1 μm in width extended from the tip of the large crack. Cracks of this type were not observed in uncycled specimens, suggesting that cycling introduced cracking throughout the body of the specimen. This observation supports

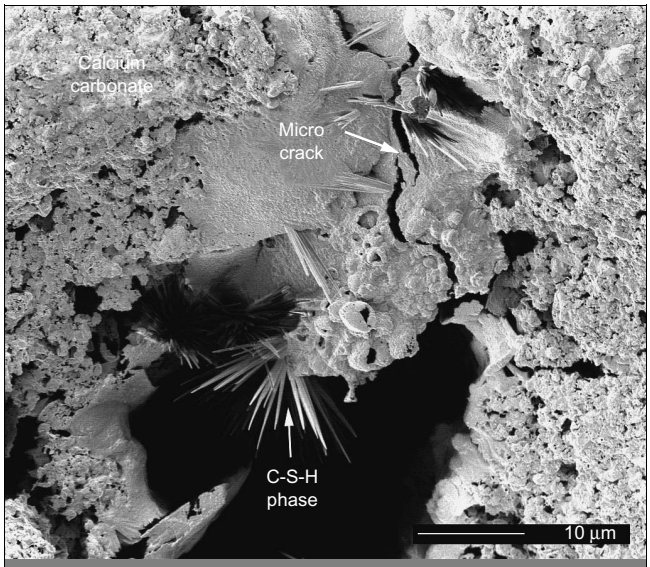

Fig. 15. Ion-induced electron image of stress-cycled lime mortar showing evidence of microcracking at the tip of a large shrinkage crack

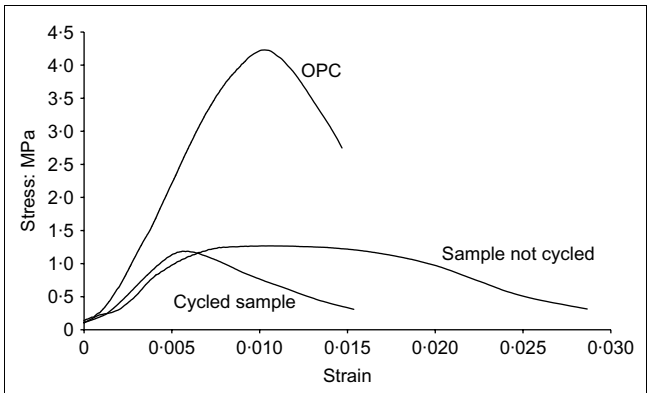

Fig. 16. Comparison of stress–strain curves obtained from 1:2 natural hydraulic lime (NHL3.5):sand mortar specimens and a 1:6 ordinary Portland cement (OPC):sand cement mortar specimen

the observed differences in response, in particular the energy absorbed during failure.

3.3. Comparison with ordinary Portland cement

Typical stress–strain curves for cycled and uncycled lime mortars and a 1:6 OPC are shown in Fig. 16. Similar specimen geometries, preparation and testing procedures were used to manufacture the OPC samples yet the ultimate stress level for the OPC was more than three times higher than that of the lime mortar. However, the modulus of OPC was approximately double that of the lime-based mortars such that stress levels in the OPC corresponding to the lime mortar ultimate stress occurred at approximately half the developed strain. One consequence of this is that for strained structures the resulting level of stress in a brick or block bedded in lime mortar would be correspondingly less than in an equivalent Portland cement mortar.

Although this may not constitute plastic behaviour in the true sense, it suggests that lime mortar structures have a greater tolerance to displacement without displaying cracking on the macro scale—although it is assumed that part of the behaviour exhibited depends on the formation of microcracks during

loading sequences. In addition, the autogenous healing phenomenon exhibited by lime mortars suggests that forms of construction using lime are able to accommodate successive displacements over a period of time without gross cracking, meanwhile regaining strength and retaining structural integrity.

Autogenous healing is generally described as the reprecipitation of calcium carbonate within cracks. A Portland cement consists of hydrated silicates that are insoluble in water and therefore could not undergo such a process. Although it is true that cement powder contains calcium hydroxide and calcium hydroxide is formed during the hydration of some clinker phases, the very high proportion of clinker phases which react with lime during hydration within cement ensures that no significant amount of calcium hydroxide or carbonate remains at the end of setting. OPC normally sets within days or weeks compared to limes which take weeks, months, years or decades, depending on geometry and ability of carbon dioxide to diffuse into the structure. The presence of water vapour is also an important factor influencing carbonation. It is unlikely that OPC-based masonry has the ability to undergo autogenous healing in the same way as lime mortar.

4. CONCLUSIONS

During stress cycling of lime mortar, energy is adsorbed by the formation of microcracks. No significant reduction in compressive stress was observed in specimens cycled up to 40 times. A reduction in energy absorbed to the point of ultimate stress was observed from the stress–strain curve.

Deformation of the mortar was linear with the exception of a small amount of plastic deformation immediately prior to the point of ultimate stress.

The increase in compressive strength of the aged mortar is attributed to: (*a*) the increase in the rate of carbonation (transformation of portlandite to calcite), and (*b*) hydration of C_2S (C_2S is the major hydraulic phase in NHL).[8]

ACKNOWLEDGEMENTS

The authors wish to thank the EPSRC and DTI for supporting this work, Hydraulic Limes Ltd for supply of materials and Castle Cement for the X-ray fluorescence analysis of the natural hydraulic lime used.

REFERENCES

1. Holmes S. and Wingate M. *Building with Lime, A Practical Introduction* (revised edition). ITDG Publishing, London, 2002.
2. Allen G. C., Allen J., Elton N., Farey M., Holmes S., Livesey P. and Radonjic M. *Hydraulic Lime Mortars for Stone, Brick and Block Masonry*. Donhead Publishing, Shaftesbury, Dorset, 2003.
3. Radonjic M., Allen G., Livesey P., Elton N., Farey M., Holmes S. and Allen J. ESEM characterisation of ancient lime mortars. *Journal of the Building Limes Forum*, 2001, **8**, 38–49.
4. Thomson M. Properties of lime mortar, understanding the nature of lime–sand mortars. *Structure Magazine*, May 2005, 26–29.
5. El-Turki A., Ball R. J. and Allen G. C. Simulated aging of lime mortars—a mechanical property, structural and compositional study. In *Proceedings of the Heritage, Weathering and Conservation (HWC-2006) Conference, Madrid, Spain* (Fort R., Alvarez de Buergo M., Gomez-Heras M. and Vazquez-Calvo C. (eds)). Taylor & Francis, London, 2006, vol. 1, pp. 51–56.
6. El-Turki A., Ball R. J. and Allen G. C. Chemical and mechanical properties of lime-based mortar materials. *Journal of the Building Limes Forum*, 2006, **13**, 71–93.
7. British Standards Institution. *Methods of Testing Cement. Determination of Strength*. BSI, Milton Keynes, 2005, BS EN 196-1:2005.
8. Lanas J., Perez Bernal J. L., Bello M. A. and Alvarez Galindo. Mechanical properties of natural hydraulic lime-based mortars. *Cement and Concrete Research*, 2004, **34**, No. 12, 2191–2201.